remote sensing

MDPI

Article

R-IMNet: Spatial-Temporal Evolution Analysis of Resource-Exhausted Urban Land Based on Residual-Intelligent Module Network

Chunyang Wang [1,2], Yingjie Zhang [2], Xifang Wu [2,*], Wei Yang [3], Haiyang Qiang [4], Bibo Lu [1] and Jianlong Wang [1]

[1] College of Computer Science and Technology, Henan Polytechnic University, Jiaozuo 454000, China; wcy@hpu.edu.cn (C.W.); lubibo@hpu.edu.cn (B.L.); wangjianlong24@hpu.edu.cn (J.W.)
[2] School of Surveying and Land Information Engineering, Henan Polytechnic University, Jiaozuo 454000, China; 212004010020@home.hpu.edu.cn
[3] Center for Environmental Remote Sensing, Chiba University, Chiba 2638522, Japan; yangwei@chiba-u.jp
[4] Chinese Academy of Natural Resources Economics, Beijing 101149, China; hyqiang@canre.org.cn
* Correspondence: wxf2020@hpu.edu.cn

Abstract: The transformation of resource-exhausted urban land is an urgent problem for sustainable urban development in the world today. Obtaining the urban land use type and analyzing the changes in their land use can lead to better management of the relationship between economic development and resource utilization. In this paper, a residual-intelligent module network was proposed to solve the problems of low classification accuracy and missing objects edge information in traditional computer classification methods. The classification of four Landsat-TM/OLI images from 1993–2020 for Jiaozuo city (the first batch of resource-exhausted cities in China) was realized by this method. The results (overall accuracy was 98.61%, in 2020 images) were better than the comparison models (support vector machine, 2D-convolutional neural network, hybrid convolution networks; overall accuracy was 87.12%, 96.16%, 98.46%, respectively) and effectively reduced the loss of information on the edge of the ground objects. On this basis, six main land use types were constructed by combining field surveys and other methods. The characteristics and driving forces of spatial-temporal change in land use were explored from the aspect of social, economic and policy factors. The results showed that from 1993 to 2020 the cultivated land, forest land, water body and other land types in the study area decreased by 690.97 km^2, 57.54 km^2, 47.04 km^2 and 59.43 km^2, respectively. The construction land and bare land increased by 839.38 km^2 and 15.57 km^2, respectively. The transfer of land use types was mainly from cultivated land to construction land, with a cumulative conversion of 920.95 km^2 within 27 years. The driving forces of land use in the study area were analyzed by principal component analysis (PCA) and regression analysis. The spatial-temporal evolution of land use types was affected by policy changes, the level of social development and the adjustment in the economy, industry and agriculture structure. The investment in fixed assets and per capita net income in rural areas were the top two influencing factors and their cumulative contribution rate was 94.62%. The findings of this study can provide scientific reference and theoretical support for land use planning, land reclamation in mining areas, ecological protection and sustainable development in Jiaozuo and other resource-exhausted cities in the world.

Keywords: remote sensing image; convolutional neural network; land use; driving force; resource depletion

Citation: Wang, C.; Zhang, Y.; Wu, X.; Yang, W.; Qiang, H.; Lu, B.; Wang, J. R-IMNet: Spatial-Temporal Evolution Analysis of Resource-Exhausted Urban Land Based on Residual-Intelligent Module Network. *Remote Sens.* **2022**, *14*, 2185. https://doi.org/10.3390/rs14092185

Academic Editor: Ioannis Gitas

Received: 7 April 2022
Accepted: 29 April 2022
Published: 3 May 2022

1. Introduction

The dynamic information of land use/cover change (LUCC) reflects the essential characteristics of the Earth's surface [1]. With the development of the social economy, LUCC has become the main form of showing human activities in the natural ecological environment [2], and land use-related issues also appear in large numbers, such as loss

and illegal occupation of arable land, soil pollution, rural residential land sprawl and so on. LUCC may affect the primary conditions for sustaining livelihoods and the balance of ecosystems, such as food production, climate regulation and biodiversity [3–5]. It has attracted the attention of more and more national governments and international organizations. Therefore, the monitoring of LUCC and the analysis of its causes have become a hot topic.

Firstly, in the process of land use type surveying, the traditional survey methods need to invest a lot of workforce and material resources, which is not conducive to efficient monitoring [6]. Secondly, the long work cycle often makes the survey results lag behind, which means it is difficult to meet the rapid development of the social economy. In recent years, remote sensing technology has developed rapidly, with the characteristics of all-day observation and rapid imaging. Randazzo et al. used maximum likelihood, minimum distance, Mahalanobis distance and spectral angle mapping to analyze sentinel-2 images from a small beach in the province of Messina; it is believed that the information about surface coverage can be obtained by LULC mapping of images [7]. Wasniewski et al. used a random forest algorithm for pixel-based land cover classification in Lodz Province, central Poland, and obtained good results [8]. Through the observation of land cover, remote sensing data are widely used to identify land use type [9]. The correct interpretation of remote sensing data has become the focus of work, and the development of computer programs has facilitated the interpretation. The automatic classification of remote sensing images can be realized quickly by using machine learning methods [10]. Land classification by computer technology instead of manual survey and visual interpretation has become a new trend. For example, the support vector machine has an advantage over traditional methods in the classification of remote sensing images [11]. After principal component analysis of the extracted features, land classification is implemented using maximum likelihood, which improves efficiency and achieves good accuracy [12]. Furthermore, classification accuracy is further improved by fusing 26 variables for the random forest method [13].

However, the above methods are shallow learning methods, which have some shortcomings such as weak noise suppression ability, limited feature description ability, poor generalization and so on [14–16]. They cannot satisfy a higher level of need. The appearance of deep learning [17–22] makes it possible to solve the above problems. It has the advantages of high classification accuracy, strong characteristic learning ability and good robustness, and can overcome the defects of traditional methods [23–30]. By introducing a residual connection into 2D-CNN, a deeper level convolution network is constructed, and the accuracy is improved compared with the original 2D-CNN [31]. Furthermore, the fusion squeezed excitation net (FuSENet), which selectively emphasizes the information feature and suppresses the noise information, also achieves a higher classification effect [32]. Although the existing convolutional neural network methods have performed well to a certain extent, they still have some shortcomings, such as the loss of edge information due to multiple downsampling operations and impact on the quantitative analysis; the convolution kernel with fixed size, shape and weight in the convolution network cannot adapt to the variable geometric features of all remote sensing images [33]. Currently, researchers are starting to introduce the graph convolution network (GCN) into remote sensing image classification to obtain more efficient models. Qin et al. applied the convolution model to hyperspectral image classification, realized cooperative training of labeled data and unlabeled data by using a regular constraint, and achieved higher accuracy than traditional convolution [34]. Wan et al. proposed a model based on dynamic graph and graph convolution, and improved the model accuracy based on multi-scale [35]. The above convolution models are simple and cannot deal with the geometric changes in the target region of hyperspectral images flexibly. Therefore, there is still much room for further improvement.

Regarding the driving forces of land use change, previous studies mainly focused on the analysis of the social factors and natural factors, such as population, economy, policy, as well as temperature, precipitation, earthquakes, fires, floods and sudden natural

disasters. In the tourist city of Pingtan Island, its special urban expansion policy played an important role in land use change [36]. The different time periods of subway construction had different influences on the surrounding land change [37]. Through selecting seven land use types as species variables and using highly correlated socio-economic indicators as environmental variables, Jiang et al. concluded that the largest factor affecting their land change is the total amount of retail sales of social consumer goods [38]. Yu et al. used the soil and water assessment tool (SWAT) model to study the impact of climate change on the evolution of wetlands in the Xiliao River Basin [39]. Spatial factors such as the distance between roads and residential areas, and natural disaster factors such as fire also affected land use change [40]. Chirwa et al. examined the socio-economic drivers of land cover change in terms of agricultural expansion, population growth and illegal logging [41]. Imberno et al. used an econometric model to analyze cropland in different regions and found that population was the main factor influencing cropland change [42]. In Puxian county of the Loess Plateau, the policy of returning farmland to forests was the main driving force affecting the spatial and temporal changes in land [43]. The above studies have obtained rich results, which provide valuable experiences for the follow-up study on the driving factors of land cover change and land development in the study area.

Socio-economic and policy changes are considered as the important determinants of land use change [40]. Jiaozuo is neither an economically developed area dominated by human factors, nor an ecologically fragile area with few social activities, but a city in transition from "resource depletion" to "green tourism". Convolutional neural networks have some advantages in the classification of remote sensing images, and residual links can solve the problem of gradient vanishing in deep networks. In such a context, in order to save costs and ensure the accuracy of the quantity of each land use type, the residual-intelligent module network was constructed to classify the remote sensing images in the study area. This method takes a 3D convolution network as the main body and introduces the famous “residual link” structure. The “intelligent module” adaptively recalibrates the characteristic responses between channels by establishing interdependencies between channels in each convolutional layer. On this basis, the spatial-temporal change in land use and its driving factors in Jiaozuo were analyzed. The research results can provide a valuable reference for land policy making and sustainable development of land resources during the urban transition period in Jiaozuo.

2. Materials and Methods

2.1. Study Area

Jiaozuo City (35°10′–35°21′ N, 113°4′–113°26′ E) is located in the northwestern part of Henan Province, People’s Republic of China, and has a long history as a major area of early Chinese activities. Covering an area of about 4071.1 km^2, Jiaozuo has a permanent population of about 3,521,100 (7th national population census, 2020). The territory has a relatively complete range of landforms, ranging from the foot of the North Taihang Mountains River to the banks of the South Yellow River, followed by mountains, hills, plains and tidal flats. The types of land resources developed and utilized in the city are cultivated land, forest land, industrial and commercial land, traffic land, housing land and so on. Jiaozuo has a temperate continental monsoon climate, with ample sunshine conditions, four distinct seasons. The annual average temperature is ranging 12.9 °C–14.7 °C, the annual average sunshine time is 379 h, the solar and thermal resources are sufficient, the annual average precipitation is about 650 mm, which can meet the growth of wheat, corn and other crops [44]. In addition, Jiaozuo is rich in mineral resources, (mainly coal) and is one of China’s top 10 coal and three fire clay bases.

In March 2008, The National Development and Reform Commission of the People’s Republic of China issued the “Notice on Printing and Distributing the List of the First Batch of Resource-Exhausted Cities” (no. 712, Development and Reform Office, 2008); Jiaozuo was listed as the country’s first resource-exhausted city [45].

In recent years, Jiaozuo has struggled to transform its status as a resource-exhausted city. With the vigorous implementation of environmental protection and green development policies, the tertiary sector of the economy has developed vigorously, the air quality has gradually improved and the emission of polluting gases has been significantly reduced. Good results have been achieved in the reclamation of coal mining subsidence areas and the ecological management of mines. Figure 1 shows the administrative location map of Jiaozuo and the remote sensing true color map based on a Landsat/OLI image in 2020.

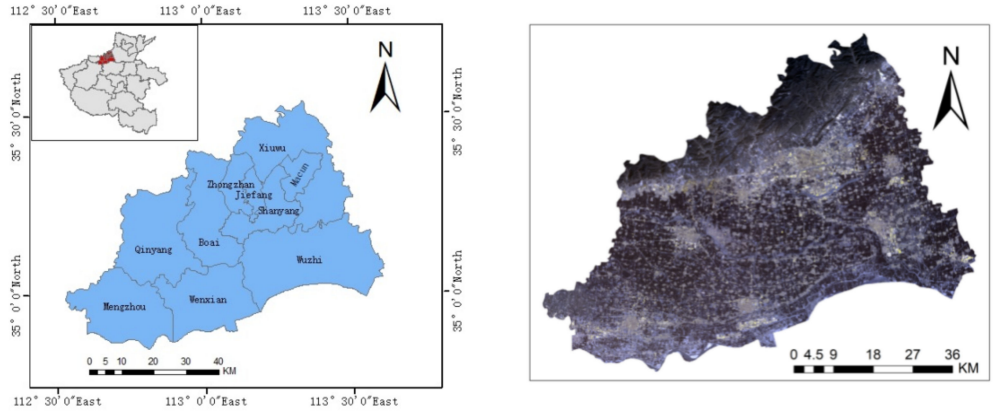

Figure 1. Location and satellite image of the study area: (**a**) Map of Jiaozuo; (**b**) True Color Image of Jiaozuo.

2.2. Data Source

In this study, four periods of Landsat remote sensing images (1993, 2003, 2011 and 2020) were collected. The resolution was 30 meters and the cloud coverage was less than 5%. Data were from geospatial data cloud sites, http://www.gscloud.cn/search (accessed on 15 March 2021). Since the study area has short sowing periods in June and October, the cultivated land is exposed. This can distinguish the farmland from other vegetation and has no obvious impact on the classification of other land features. As a result, images from both periods were selected. Four remote sensing images were preprocessed by radiometric calibration, atmospheric correction, geometric correction and image registration [46]. The study area was extracted using vector boundaries, and the socio-economic data were obtained from the Jiaozuo Statistical Yearbook.

In the selection of training samples, firstly, according to the national land cover classification standard [47,48] and the actual situation of the study area, there were six land use types. Woodland (refers to land where trees, bamboos, shrubs and coastal mangroves grow), bare land (refers to land with little vegetation cover), cultivated land (refers to land where crops are grown), construction land (refers to land where buildings and structures are built), water body (refers to land waters, mudflats, ditches, swamps, hydraulic structures, etc.) and other land (other than the above land types) were determined by means of visual interpretation. The symbol of remote sensing image interpretation is shown in Table 1. Then, a certain size of patch was radially extended to the surrounding area by a pixel point on the original image, and the land type of the selected center pixel was taken as the land type label of the patch. Each type of land use type had more than 100 samples. In order to reduce the spectral variability of similar land features caused by surface slope and the orientation of the sensors, the NDVI (Normalized Difference Vegetation Index), NDWI (Normalized Difference Water Index) and NDBI (Normalized Difference Building Index) were used as characteristic variables to improve the classification accuracy. The calculation method of the three indexes is shown in Equations (1)–(3). Finally, the present land use map in Jiaozuo combined with field survey was used as a reference for post-classification processing.

$$NDVI = (NIR - R)/(NIR + R) \quad (1)$$

$$NDWI = (G - NIR)/(G + NIR) \quad (2)$$

$$NDBI = (SWIR - NIR)/(SWIR + NIR) \quad (3)$$

where: Equations (1)–(3) are the calculation formula of *NDVI*, *NDWI*, *NDBI* in turn. *NIR* is near-infrared band, *R* is red band, *G* is green band, *SWIR* is short-wave infrared band.

Table 1. Remote sensing interpretation signatures of land use types in Jiaozuo city.

Land Use Type	Remote Sensing Image Characteristics	Interpretive Marker
Woodland	Appearing red in the Nir, R and G bands	Mostly in the northern mountains.
Bare land	Bright color in true color band	Distributed on the periphery of construction land and cultivated land.
Construction land	Dark purple in the Nir, R and G bands	Mostly surrounded by arable land.
Cultivated land	Appearing red in the Nir, R and G bands	Distributed throughout the study area, the largest area.
Water body	Blue or black in in the Nir, R and G bands	Linear distribution, the characteristics are obvious.
Other land	Mostly brown in true color band	Concentrated in mountainous and overgrown areas.

2.3. Methods

In this manuscript, a mixed convolution network model based on the fusion of super-pixels is proposed for land classification, which aims to overcome the problems of low classification accuracy and missing edge information.

2.3.1. Hybrid Convolution Network Incorporating Super-Pixel Segmentation

The convolutional neural network consists of an input layer, a convolution layer, a pooled layer, an activation function and a fully connected layer. The image is fed into the model through the input layer, and the convolution core in the convolution layer checks the input data to extract the features. The extracted features are sampled in the pool layer to remove the feature redundancy and retain the important features. Finally, the activation function is adopted and the weighted result is obtained by back propagation through the weight value. The following is how feature extraction works

$$V_{ij}^{xyz} = f\left(\sum\sum_{p=0}^{P_i-1}\sum_{q=0}^{Q_i-1}\sum_{r=0}^{R_i-1} W_{ijm}^{pqr} V_{(i-1)m}^{(x+p)(y+q)(z+r)} + b_{ij}\right) \quad (4)$$

where i represents the current number of layers; V_{ij}^{xyz} represents the output of the j-th feature map (x, y, z) of the i-th layer; m is the number of feature maps connected to the $i-1$-*th* layer; W_{ijm}^{pqr} is the weight of the (p, q, r) position in the m-th feature; b_{ij} is the bias; f is the activation function. P_i, Q_i and R_i are the length, width and height of the 3D convolution kernel.

A super-pixel is a small area composed of a series of adjacent pixels with similar color, brightness, texture and other characteristics. These small areas retain useful information about the image. In general, the boundary information of the object in the image is not destroyed. The complexity of image processing can be effectively reduced by using a small number of super-pixels instead of a large number of pixels to express image features [49].

In this method, Simple Linear Iterative Clustering (SLIC) algorithm is used to segment super-pixel image, which is based on K-means idea. In the process, a 5-dimensional vector (L, A, B, x, y) is composed of (L, A, B) color values and (x, y) coordinates of each pixel, and then a distance metric is constructed from the 5-dimensional eigenvector.

Firstly, the algorithm generates K seed points, calculates the similarity of pixels in a particular area with the seed as the center, classifies each pixel and obtains K initial super-pixels. Then, it calculates the average vector value of the pixel points in the K super-pixels, and obtains the K cluster centers again. Then, the similarity of pixels in a certain size area centered on the seed is calculated, and each pixel is classified to obtain K super-pixels,

update the cluster center and iterate again. Finally, the K cluster centers do not change and achieve convergence. The algorithm accepts a parameter K, which is used to determine the number of pre-segmented super-pixels. Assuming the original image has N pixels, then each super-pixel is divided into about N/K pixels. The side length of each super-pixel is approximate

$$S = [N/K]\hat{}0.5 \quad (5)$$

The algorithm takes a cluster center every S pixel and uses the $2S \times 2S$ around the cluster center as the search space. This procedure is used to identify more similar points in the region with the cluster center, and finally complete the super-pixel segmentation operation.

Then, the result of super-pixel segmentation is convolved to obtain a feature map of $W \times H \times B \times C$ (W and H are the width and height of the feature graph, respectively, B is the number of bands, C is the number of channels). By merging the B dimension and the C dimension to form a volume of $W \times H \times (B \times C)$, the two-dimensional convolution layer is input. Finally, the feature graph is transformed into a one-dimensional vector by flatten layer and the class information is output by the Softmax activation function. Figure 2 shows the schematic diagram of the entire model.

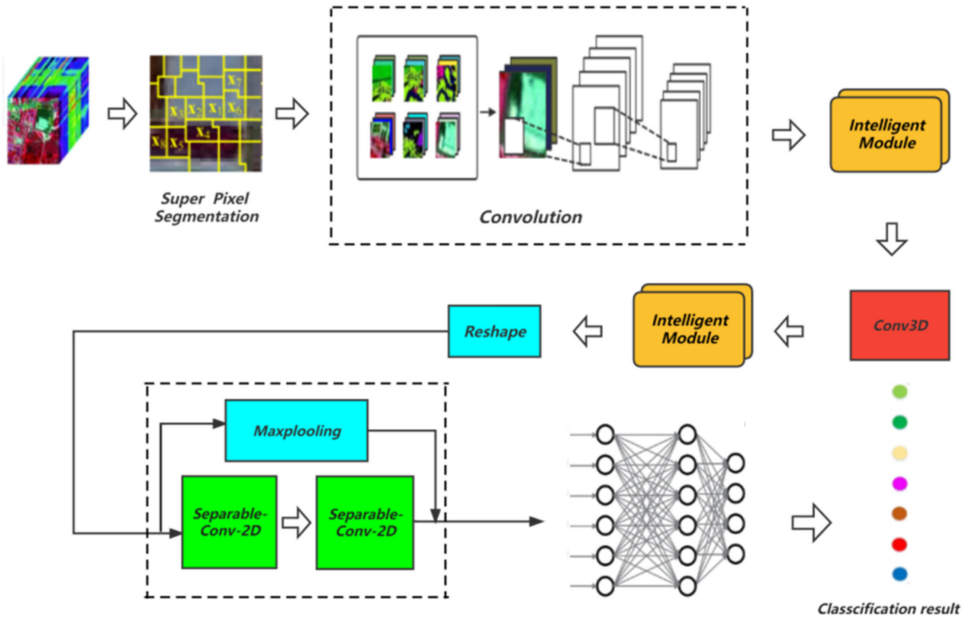

Figure 2. Schematic diagram of model structure.

"Intelligence module" consists of two convolution layers and a residual link. The role is to adaptively recalibrate the feature responses between channels by establishing interdependencies between channels at each convolutional layer. It can selectively emphasize the informative feature and suppress the noise feature, making the model perform better. It is well known that when the number of network layers increases to a certain number, the training accuracy will not continue to increase with the network layer number but will decrease. Therefore, a residual link is introduced (Figure 3). By adding a jump connection network structure between the input and the output, the output can obtain the original data of the input, solve the problem of gradient vanishing and further improve the learning performance of the network. The structure is shown in Figure 4.

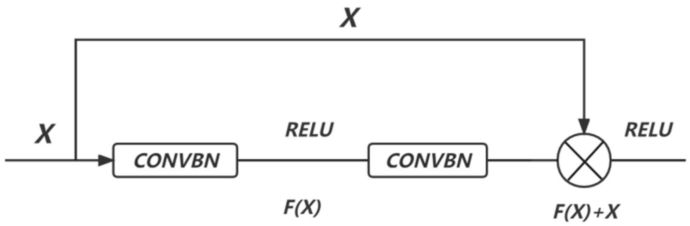

Figure 3. Residual Learning Module.

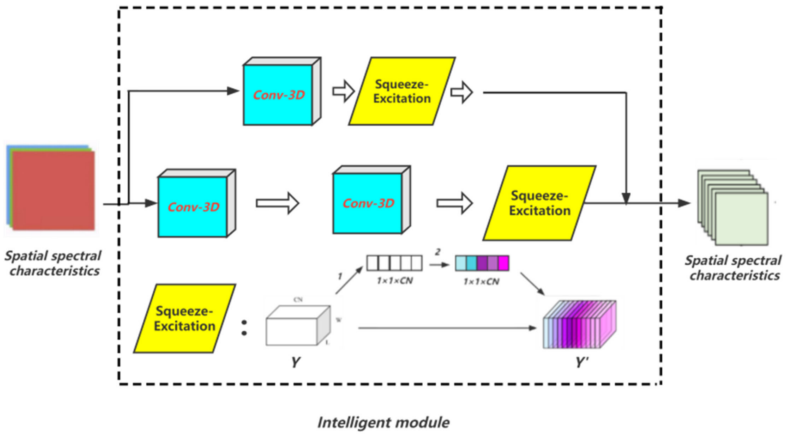

Figure 4. Structure diagram of intelligent module.

In Figure 3, x is the input of the residuals module; $H(x)$ is the output of the residuals learning module with short connections; $F(x)$ is the output of the residuals without short connections. *CONVBN* represents convolution and batch normalization operations, and *RELU* defines activation functions. The input–output relationship of the residual learning module is as follows

$$H(x) = F(x) + x \tag{6}$$

where $H(x)$ can be understood as the sum of the input x and the residual mapping $F(x)$.

The yellow operation results from the normal convolution Y, (assuming the size is $W \times H \times CN$). The first step is to create a branch for "Squeeze" operation. The featured graph is transformed into an actual number and the dimension into a $1 \times 1 \times CN$, similar to the pooling operation under the global sensory field. The number of channels in the process remains constant. This is followed by the second step, the "Excitation" operation. It generates weights for each channel and applies them to the original feature channel. The size of the output Y' is still $W \times H \times CN$, but the importance of each channel has changed. In this way, some feature channels can be reused. This module can improve the learning ability of the model, and only a few parameters need to be calculated. In the convolution part of the whole model, the dilated convolution is used to expand the receptive field and it can reduce the information loss caused by the downsampling operation.

The reason for choosing this model instead of the traditional automatic computer image classification method is that:

(1) The traditional machine learning classification method belongs to the shallow level model, which has simple structure, the weak ability of noise suppression and the limited ability of feature description. Therefore, traditional methods often have low classification accuracy and cannot meet the needs of follow-up research.

(2) The standard convolutional neural network model cannot adapt to the geometric changes in remote sensing images because of the loss of small and linear objects in the image due to the downsampling. The result of classification cannot be used to calculate

the quantitative relationship of land use types, and it is not helpful to describe the spatial-temporal change in land use. Thus, it is not suitable for Jiaozuo, where the land use types are complex and fragmented. Consequently, the above method was selected in this study.

2.3.2. Other Related Methods

Land use dynamic index: Under the comprehensive influence of natural and social factors, the quantity change of each land use type is different in different periods. Land use dynamic index can quantitatively reflect the rate of regional land use change and the difference in land use change in different periods. It plays an active role in predicting future land use change trends [50]. One of the land use dynamic indices of the calculation Equation (4) is as shown

$$K = \frac{N_b - N_a}{N_a} \times \frac{1}{T} \times 100\% \tag{7}$$

where K is the dynamic of a particular land use type; N_a and N_b are the area at the beginning and end of the study for a particular land type, respectively; T is the study period.

Information entropy of land use structure: The information entropy of land use structure can reflect the orderliness of the land use system. The higher the entropy value, the weaker the orderliness, and the system is unstable and unfavorable to development. The calculation equations are as follows

$$H = -\sum_i^n P_i \ln P_i \tag{8}$$

$$E = H / \ln n \tag{9}$$

$$D = 1 - J \tag{10}$$

where H is the entropy of land use structure information; E is the degree of equilibrium, reflecting the degree of equilibrium of land use in a region; D is the degree of dominance, reflecting the extent to which one or several land use types dominate the land types in the region; P_i is the proportion of a land use type in the whole study area; the sum of equilibrium degree and dominance degree is 1 [51].

Land use change maps and transfer matrix: This can be used to study the mutual transformation and spatial distribution of land use types, and reveal the law of its evolution. We use the map algebra method to obtain the land use change mapping in a specific period, and, furthermore, obtain the land use transfer matrix that can quantitatively reflect the source and destination of each land use type, and its equations are

$$M = M_1 \times 10 + M_2 \tag{11}$$

$$S_{ij} = \begin{bmatrix} S_{11} & S_{12} & \cdots & S_{1n} \\ S_{11} & S_{11} & \cdots & S_{2n} \\ \cdots & \cdots & \cdots & \cdots \\ S_{n1} & S_{n2} & \cdots & S_{nn} \end{bmatrix}, D_i = \sum_{j=1}^n S_{ij} - S_{ii}, D_j = \sum_{i=1}^n S_{ij} - S_{jj} \tag{12}$$

where M is the land use change mapping raster within the study section; M_1 and M_2 are the raster values of land use mapping attributes at the beginning and end of the study period, respectively; S_{ij} represents the land type i to the land type j of the area. D_i represents the study period; i , the area of land use reduction by land type; D_j represents the area of j the area of increased type of land use.

3. Results

The above model was used to classify land use in the four phases of images in the study area and compared with existing classification models such as SVM (support vector machine), 2D-CNN(2D convolutional neural network), and hybridSN (hybrid convolutional network). The overall accuracy (OA) and kappa coefficients of different models based on the 2020 dataset are shown in Table 2.

Table 2. Classification precision table of each model.

	SVM	2D-CNN	HybridSN	R-IMNet *
OA/%	87.12	96.16	98.46	98.61
Kappa	0.82	0.94	0.97	0.98

Note: * denotes the model of this paper, IM refers to intelligent module.

Based on the classification results of the model, the field survey is carried out to correct the doubtful points of the results. The final accuracy evaluation results are shown in Table 3. It meet the requirements of follow-up analysis.

Table 3. The classification accuracy in the different years.

	1993	2003	2011	2020
OA/%	94.35	98.49	99.09	98.61
Kappa	0.92	0.98	0.99	0.98

To verify the advantages of this model in reducing the information loss of linear objects and objects edge, we selected an area with more road information based on the image of Jiaozuo in 2020. The results were compared with SVM, 2D-CNN and HybridSN, as shown in Figure 5.

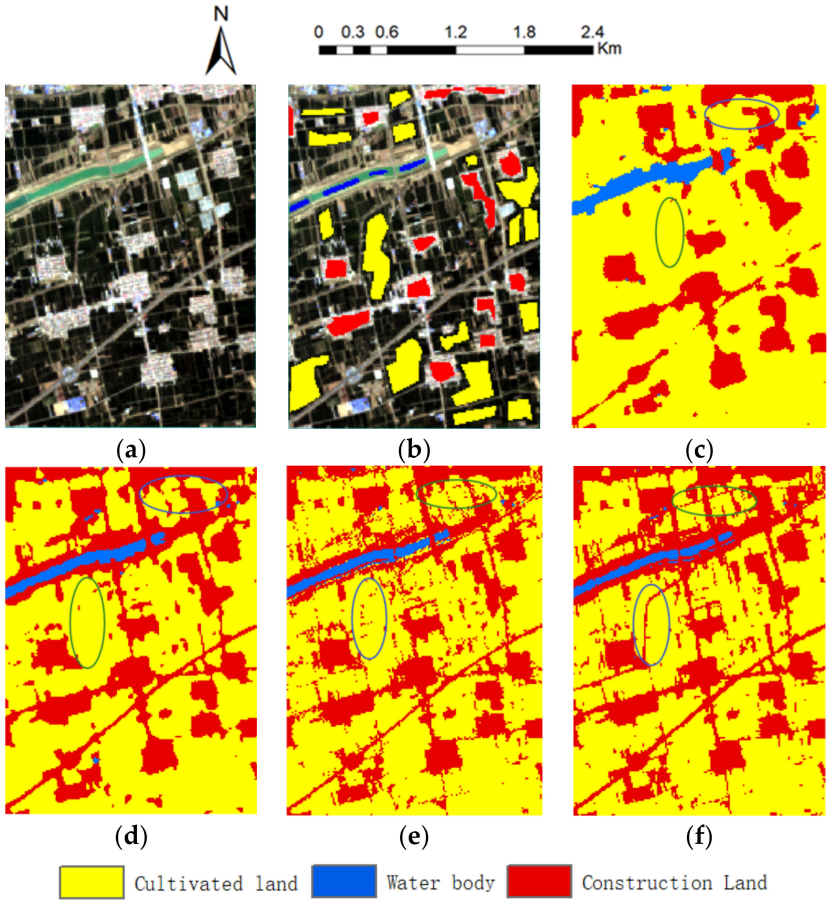

Figure 5. Classification maps of typical region. (**a**) True Color Image; (**b**) Land use ground truth; (**c**) 2D-CNN; (**d**) HybridSN; (**e**) SVM; (**f**) R-IMNet.

It can be seen that the poor classification of the 2D-CNN and HybridSN algorithm, the information loss of the edge information of the objects and the line-like small objects were very severe. In particular, 2D-CNN causes the most significant loss of the edge

information of ground objects. As shown in the Ellipse Mark, the road information was almost completely lost, and the boundary between the construction land and the cultivated land was blurred. The classification results from the HybridSN model were improved, but there was still a gap compared with the model in this paper. In addition, SVM performed better than 2D-CNN and HybridSN in controlling the confusion of the edge information of objects, but it also showed a slight loss of road information. However, SVM was inferior to R-IMNet in noise control. Overall, R-IMNet has more advantages in reducing information loss of linear objects, objects edge and noise control.

3.1. Land Use Change

The land use classification maps of Jiaozuo City in 1993, 2003, 2011 and 2020 are shown in Figure 6. The map clearly reflects the land use patterns of the study area in different periods. It can be seen that the land use types in the study area changed significantly in the four periods. Over nearly 30 years from 1993 to 2020, the area of construction land increased significantly, and the area of cultivated land decreased continuously. Each land use type evolved alternately, among which a large amount of bare land appeared in 2011, the area of water bodies and other land uses changed relatively slowly.

In order to reflect the quantitative relationship and change intensity of land use types, the basic data of land use in the study area were acquired by Arcgis10.2 software based on the results of the 4-stage classification. Based on the Equations (7)–(10), the dynamic index of land use type change, the information entropy of land use structure, the degree of equilibrium and the degree of superiority were obtained. The results are shown in Table 4.

From Table 4, the basic landscape of Jiaozuo included woodland, cultivated land and construction land from 1993 to 2020, accounting for 90% of the total area in the four periods. Figure 7 showed the proportion of land use structures in the four periods in the study area. The cultivated land (red part in Figure 7) was the main type of land use. The area proportion reached 56.12%, 54.32%, 45.70% and 38.74%, respectively, and ranked first in the study area. Except for the special situation in 2011, bare land was distributed sporadically among other land use types, and water body was mainly distributed among the rivers in the southern part of the study area, accounting for a small proportion, 2.18%, 1.37%, 1.48% and 1%, respectively.

From 1993 to 2020, the area of bare land and construction land showed an increasing trend, increasing by 15.57 km^2 and 839.38 km^2, respectively. Construction land area increased by a large margin, reaching 145.52%, and its growth rate was 5.39%. During the 27 years, the change rates of bare land at three time points were 9.73%, 13.95% and −7.64%, showing a rapid increase followed by a sharp decrease. During 2011–2020, the change rate of bare land was −7.64%, with a trend of maintaining a continuous decline. Woodland, cultivated land, water body and other land decreased by 57.54 km^2, 690.97 km^2, 47.04 km^2 and 59.43 km^2, respectively. Among them, the water body decelerated fastest, and reduced the amplitude the most, −2.01% and −54.28%, respectively. During the study period, the cultivated land area maintained a decreasing trend, the rate of reduction was −0.32%, −1.98% and −1.69%, respectively, and the total area ratio decreased by 17.38%. However, the areas of woodland, water body and other land all experienced brief increases.

From the information entropy of land use structure, this increased from 1.24 to 1.30 in Jiaozuo from 1993 to 2003. It indicated that the land use in the study area was in a state of rapid change and the instability of the whole system increased during this period. By 2011, the entropy had risen to 1.33. The increase in the information entropy was mainly due to the rapid development of Jiaozuo City over the past 18 years, with a high degree of disorder in various industries. In 2020, the entropy value decreased to 1.31, but it was still higher than that in 1993 and 2003. This was due to the initial effect adjusting the industrial structure in Jiaozuo, the standardization of land use and the partial orderly development of the fundamental land use change [52,53]. Between 2003 and 2020, the entropy dominance of the study area was less than 0.3, reflecting the low power of the dominant local utilization type—cultivated land. Throughout the study period, the land use equilibrium degree of

Jiaozuo was kept at about 0.7. This indicates that the homogeneity of the land use structure was at a high level. The regional landscape advantage was not different, and there was no apparent advantage landscape type.

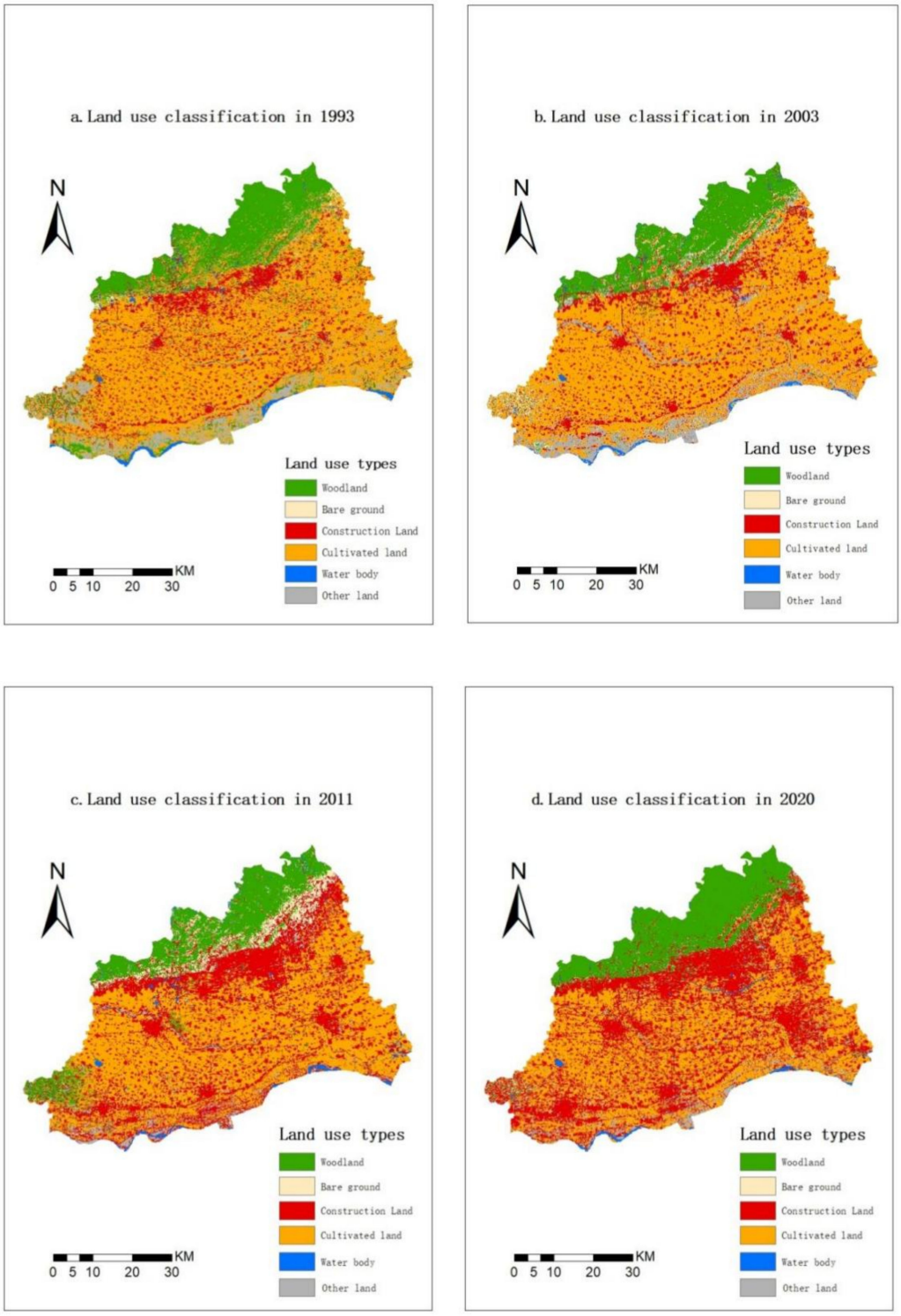

Figure 6. Land use maps of Jiaozuo city.

Table 4. Statistical table of land type change data from 1993 to 2020.

	Wood Land	Bare Land	Construction Land	Cultivated Land	Water Body	Other Land	Entropy Value	Degree of Equilibrium	Degree of Dominance
1993 Acreage /km^2	776.79	51.15	576.80	2230.44	86.66	252.28	1.24	0.69	0.31
Percentage /%	19.55	1.29	14.51	56.12	2.18	6.35			
2003 Acreage /km^2	592.68	100.94	635.28	2158.85	54.48	431.85	1.30	0.73	0.27
Percentage /%	14.91	2.54	15.99	54.32	1.37	10.87			
1993–2003 Land use dynamics	−2.37	9.73	1.01	−0.32	−3.71	7.12	-	-	-
2011 Acreage /km^2	600.54	213.61	1161.34	1816.23	58.71	123.66	1.33	0.74	0.26
Percentage /%	15.11	5.38	29.22	45.70	1.48	3.11			
2003–2011 Land use dynamics	0.16	13.95	10.35	−1.98	0.97	−8.92	-	-	-
2020 Acreage /km^2	719.25	66.72	1416.18	1539.47	39.62	192.85	1.31	0.73	0.27
Percentage /%	18.10	1.68	35.64	38.74	1.00	4.85			
2011–2020 Land use dynamics	2.20	−7.64	2.44	−1.69	−3.61	6.22	-	-	-
1993–2020 Land use dynamics	−0.27	1.13	5.39	−1.15	−2.01	−0.87	-	-	-

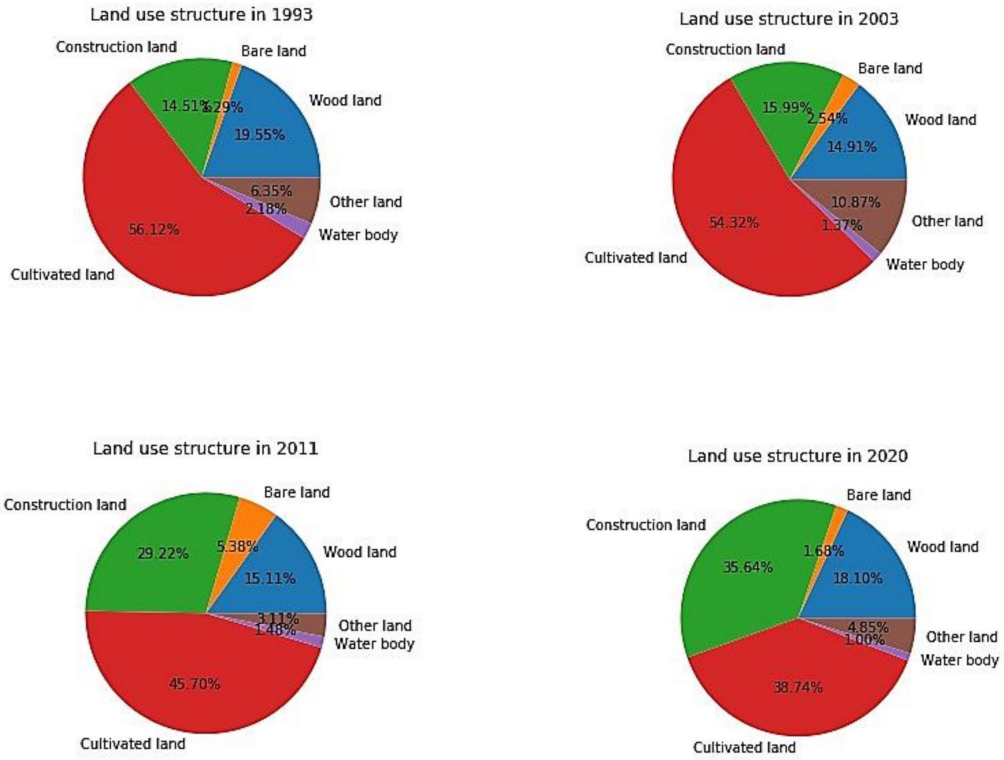

Figure 7. Land use structure in Jiaozuo.

3.2. Land Use Change Maps and Transfer Matrix

To further reflect the spatial change and quantitative relationship of the land use types in the study area, the maps of land use transition matrix and its change were made in 1993–2003, 2003–2011 and 2011–2020 according to formulas (11) and (12). The results are shown in Table 5, Table 6, Table 7 and Figure 8. In the three study periods, there were 36 types of map units. That is, every kind of utilization experienced a process of turning in and turning out. The total areas transferred were 1317.93 km^2, 1237.91 km^2 and 1237.35 km^2, respectively. The transfer between cultivated land and construction land was the biggest. Although the area of water body varied considerably compared with itself, it only accounted for 1% to 2% of the study area. Thus, it was not analyzed.

Table 5. Land use transfer matrix of Jiaozuo City from 1993 to 2003 (km^2).

	Wood Land	Bare Land	Construction Land	Cultivated Land	Water Body	Other Land	Roll-Out Total
Wood land	495.50	42.05	48.70	98.71	9.98	81.84	281.28
Bare land	15.08	3.15	6.59	18.30	0.28	7.71	47.96
Construction land	29.10	10.06	330.68	160.76	6.99	39.21	246.12
Cultivated land	42.99	34.30	201.89	1729.59	15.02	206.65	500.85
Water body	4.38	0.69	29.24	10.80	21.16	20.38	65.49
Other land	5.63	10.70	18.18	140.67	1.05	76.05	176.23
Roll-in total	97.18	97.8	304.6	429.24	33.32	355.79	1317.93

Table 6. Land use transfer matrix of Jiaozuo City from 2003 to 2011 (km^2).

	Wood Land	Bare Land	Construction Land	Cultivated Land	Water Body	Other Land	Roll-Out Total
Wood land	455.40	83.98	35.14	7.03	7.99	3.14	137.29
Bare land	25.28	26.34	28.70	15.95	0.47	4.21	74.61
Construction land	15.99	14.83	539.30	48.15	8.28	8.74	95.99
Cultivated land	67.73	43.65	344.14	1641.82	13.90	47.59	517.01
Water body	6.26	1.56	21.37	2.65	18.00	4.64	36.48
Other land	29.87	43.25	192.70	100.64	10.07	55.32	376.53
Roll-in total	145.13	187.27	622.05	174.42	40.71	68.32	1237.91

Table 7. Land use transfer matrix of Jiaozuo City from 2011 to 2020 (km^2).

	Wood Land	Bare Land	Construction Land	Cultivated Land	Water Body	Other Land	Roll-Out Total
Wood land	481.44	13.52	56.29	40.51	1.34	7.44	119.10
Bare land	139.83	11.43	37.56	15.01	0.84	8.94	202.18
Construction land	68.78	19.22	881.73	120.66	9.92	61.03	279.61
Cultivated land	14.68	19.55	374.92	1317.96	6.14	82.98	498.27
Water body	9.83	0.59	21.42	6.42	16.08	4.37	42.63
Other land	4.69	2.39	44.26	38.91	5.31	28.09	95.56
Roll-in total	237.81	55.27	534.45	221.51	23.55	164.76	1237.35

As shown in Table 5, during the decade of 1993–2003, the total amount of cultivated land transferred to the other five kinds of land was 500.85 km^2. Among them, construction land and other land transfer was the most, 201.89 km^2 and 206.65 km^2, respectively. They account for more than 90% of the area transferred from cultivated land. However, during this decade, the area of cultivated land transferred in reached 429.24 km^2, while the actual area transferred out was only 71.61 km^2, and the actual transferred area of construction land was only 58.48 km^2. This was due to the slow pace of urbanization in Jiaozuo between 1993 and 2003, and the main land use types were basically in a balanced state. The actual area of forest land transferred out was the largest, ranking first in the net change of land use in the study area, with 184.1 km^2, of which 98.71 km^2 was converted into cultivated land, accounting for 53.61%. At the end of the last century, illegal quarrying, logging and blind reclamation were severe in the mountainous areas of northern Jiaozuo. This resulted in a large number of vegetation-covered mountains being exposed [54]. Although the area of cultivated land was increased, it seriously damaged the ecological environment of forest areas. Furthermore, it increases the frequency of local geological disasters, and accelerates the progress of regional ecological environment deterioration. Between 1993 and 2003, the net transfer of other land use was 179.56 km^2, mainly converted from cultivated land and woodland. It reflected that the local awareness of intensive and economic land use was not strong, and the protection of cultivated land was neglected while reclaiming and cultivating.

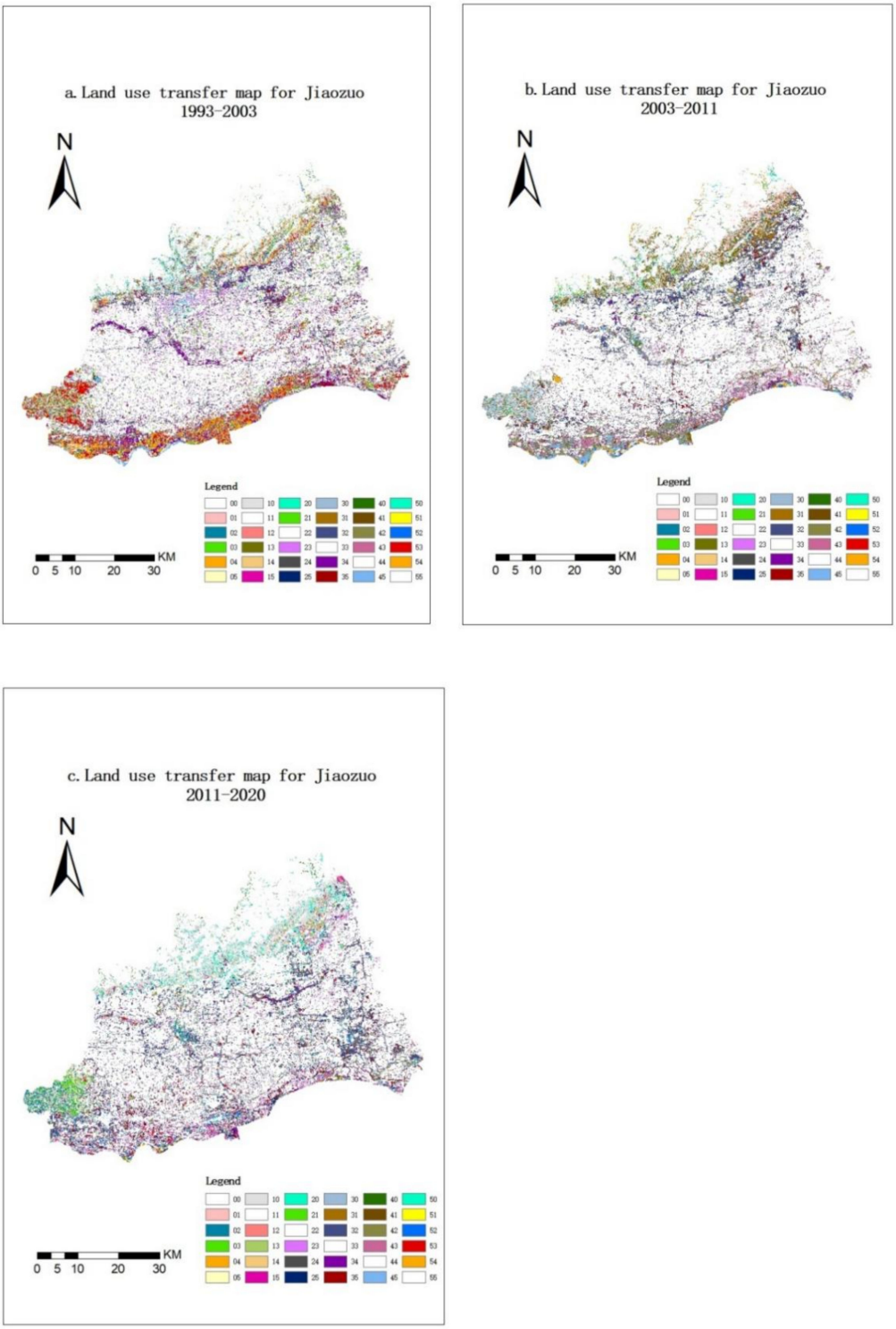

Figure 8. Land use transfer map for Jiaozuo 1993–2020.

During 2003–2011, the change in woodland was relatively moderate, while the change in construction land was the most drastic, with 622.05 km^2 transferred in and 95.99 km^2 transferred out, resulting in a net transferred area of 426.06 km^2. Its primary source was cultivated land, which was 344.14 km^2, accounting for 80.77% of the net transferred area. At the same time, the net transfer out of cultivated land and other land also reached 342.59 km^2 and 308.21km^2, respectively. This shows that in 2003–2011, the pace of urbanization in Jiaozuo accelerated and the size of cities continued to expand. With the

improvement in economic conditions, many rural self-built houses came into being, and the rural residential bases showed the phenomenon of harmful expansion, resulting in a large amount of arable land and other land being occupied in this period [55]. With the increase in the implementation time of the "Land Administration Law of the People's Republic of China" and the intensification of government enforcement, this phenomenon eased slightly. For example, from 2011 to 2020, the net area of cultivated land transferred out was 276.76 km^2, and the average annual net transfer out was 30.75 km^2. The speed and magnitude of change decreased compared with the period of 2003–2011. At the same time, from 2003 to 2011, the net transfer of bare land area was 112.66 km^2. This was because, in 2008, Jiaozuo was identified as a "resource-depleted" city and the state restricted resource exploitation. Along the Northern Mountain area, a large number of small coal mines and coal washeries were forced to close down demolition, and vacated land was not used effectively or promptly. This resulted in a large amount of bare land. With the acceleration in the urbanization process, part of the rural labor force came into the city, resulting in an amount of cultivated land and shrub orchard waste, leading eventually into bare land. In this period, the rough development of Jiaozuo led to the significant fluctuation in land use structure, and the contradiction between humans and land began to emerge.

In 2011–2020, cultivated land and construction land still changed sharply, which continued to change from cultivated land to construction land in a large amount, reaching 374.92 km^2. A large amount of bare land area was transferred out, and the leading destination was forest land. During this period, the state vigorously promoted ecological environment construction. A large number of abandoned mining areas in Jiaozuo were reclaimed and transformed, the area of woodland began to increase. In particular, in 2017, Jiaozuo was listed as a key city in the "air pollution control battle" [56], which accelerated this process, and in 2011–2020, Jiaozuo gradually shifted from rough development to high-quality development. The society's awareness of intensive and economical use of land increased, and the contradiction between humans and land began to moderate during this period.

Figure 8 shows the spatial changes in land use over the three periods in Jiaozuo; the white part of the figure is the area where the land use type did not change. The figures 0–5 in the legend represent woodland, bare land, construction land, cultivated land, water body and other land, respectively, and the figure 01 represents the part of the forest land transformed into bare land during this period and so on.

It can be seen that the most drastic changes were in the southern part along the Yellow River, the combination of mountainous areas and plains in the north, and the more populated urban areas. In addition, the main categories of utilization that have been transformed over time are reflected in the graph in much the same way as in Table 4 to Table 6.

3.3. Driving Force Analysis

Land use evolution is a complex process, and the driving factors vary in different regions. Based on reference to the relevant research combined with the characteristics of the research area, and following the drive, therefore, of the selection principle [57,58], 17 indicators in five categories of driving factors were selected: demographic factors, economic factors, agricultural structure, policy factors and at the social development level. Then, the principal component analysis and regression analysis methods were used to analyze the main driving factors of land use type evolution in the study area (shown in Table 8).

Table 8. Change index of land use driving force.

Factors	Indicators
Demographic factors	X1 total population at the end of the year, X2 non-agricultural population
Economic Factors	X3 gross regional product, X4 primary industry. X5 secondary industry, X6 tertiary industry, X7 industrial value added
Agricultural structure	X8 grain production, X9 oilseed production, X10 cotton production, X11 vegetable production, X12 total meat production
Policy Factors	X13 social fixed asset investment, X14 fiscal budget revenue, X15 fiscal budget expenditure
Social Development Level	X16 total retail sales of social consumer goods, X17 per capita net income of farmers

3.3.1. Principal Component Analysis

After standardized treatment of the 17 influencing factors, the cumulative contribution rate of principal components 1 and 2 was 94.63%. The eigenvalues were all greater than 1, which satisfies the data analysis standard. Their component loading matrixes after orthogonal rotation are shown in Table 9.

Table 9. Factor load matrix after orthogonal rotation.

Factor	Component 1	Component 2	Factor	Component 1	Component 2
X_{13}	0.995	0.056	X_4	0.923	0.341
X_{17}	0.990	0.107	X_9	0.912	0.315
X_{15}	0.990	0.111	X_8	0.856	0.322
X_6	0.989	−0.013	X_1	0.827	0.525
X_{16}	0.986	0.117	X_2	0.816	0.398
X_3	0.981	0.179	X_{11}	0.455	0.846
X_7	0.964	0.239	X_{12}	−0.073	0.940
X_{14}	0.961	0.261	X_{10}	−0.896	−0.247
X_5	0.946	0.291			

As can be seen from the table above, the load coefficients of the principal component 1 of the indicators related to the level of economic, policy and social development are all greater than 0.9. Therefore, principal component 1 can be categorized as a socio-economic development-type factor. The load coefficients of vegetable yield and meat yield in principal component 2 are relatively high, which can be concluded as agricultural factors. The land use drivers in Jiaozuo were dominated by the policy and social development levels, followed by economic factors and supplemented by agricultural factors.

3.3.2. Linear Regression Analysis

The results of the above analysis show that policy factors and the level of social development were the primary sources of land use drivers in Jiaozuo. To further analyze the relationship between the main drivers and land use evolution, the area of construction land was selected (unit: km^2). It was relatively sensitive to urbanization and economic development, as the dependent variable. Other than that, social fixed asset investment (X13 unit: 100 million yuan), per capita net income of farmers (X17 unit: yuan), fiscal budget expenditure (X15 unit: 100 million yuan), tertiary industry (X6 unit: 100 million yuan) and total retail sales of social consumer goods (X16 unit: 100 million yuan), a total of five indicators with the greatest relationship with policy and social development, were selected as independent variables for linear analysis. The sample information for the independent variables is shown in Table 10. The results are shown in Figure 9; their R^2 are all greater than 0.8, with significant effects.

Table 10. Sample Information Table For independent variables.

	1	2	3	4	5	6	7	8	9
X13	60.98	63.53	50.20	187.16	491.33	970.82	1374.04	2198.01	3064.28
X17	2238	2586	2445	3374	5326	7512	11400	14851	19374
X15	12.88	14.76	15.85	38.63	75.03	121.55	139.20	217.34	297.60
X6	57.37	55.53	72.28	131.14	219.76	289.03	423.27	721.1	1131.2
X16	54.55	65.23	75.1	118.8	180.38	321.84	494.7	698.92	873.55

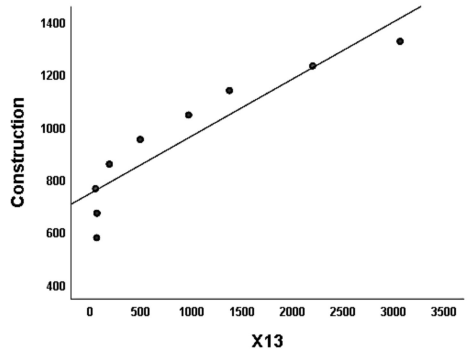

(**a**) R^2= 0.875, Y = 0.22 × x+746

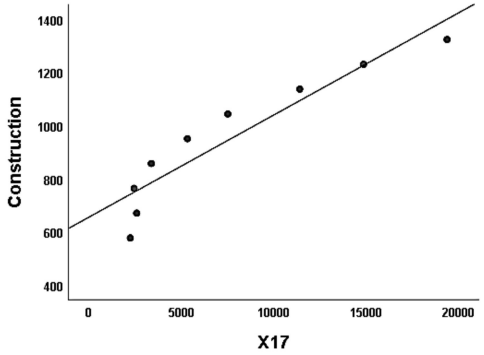

(**b**) R^2= 0.848, Y = 0.04 × x+655

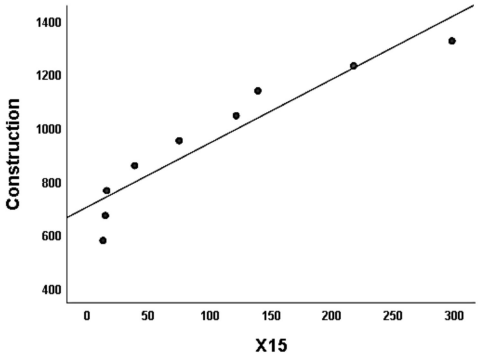

(**c**) R^2=0.887, Y = 2.39 × x+702

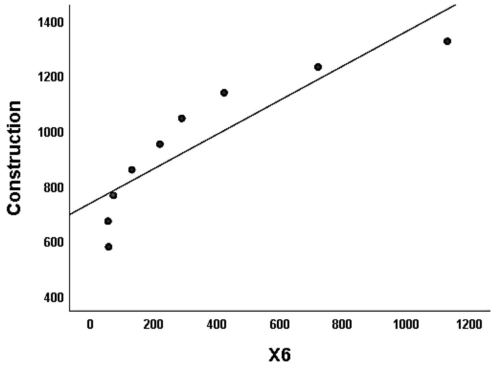

(**d**) R^2= 0.806, Y=0.62 × x+735

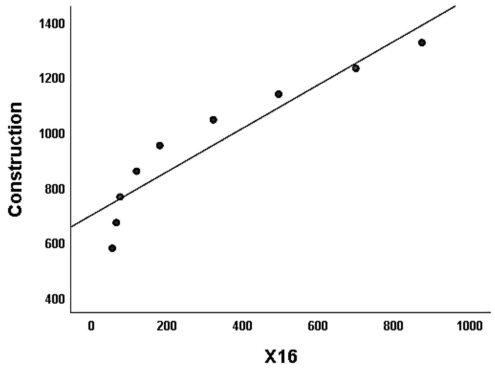

(**e**) R^2= 0.876, Y = 0.79 × x+679

Figure 9. Regression analysis model diagram.

(1) Policy implementation. The social fixed asset investment and fiscal budget expenditure increased significantly, 50 times and 25 times, respectively, from the beginning to the end of the study period. Among these is included the fixed assets investment, mainly for industrial investment, infrastructure construction and real estate investment. In contrast, the capital expenditure also increased year by year. This not only effectively drove the

rapid development of the local economy, but also directly led to the rapid increase in construction land. In recent years, Jiaozuo has tended to build green and livable cities, focusing on the quality of urban development, urban greening and the construction of urban tourism projects. At the same time, the process of urbanization has been accelerating with the development of high-tech industrial clusters and construction land area increases correspondingly.

(2) Industrial structure. In 2008, after the national "resource-depleted" cities were released, the local government began to adjust the industrial structure. The proportion of secondary industry decreased year by year, from 68.5% in 2009 to 53.6% in 2019, and some mineral mining sinkholes were transformed into unique tourist attractions. In addition, the agricultural structure also changed: farmers began to plant yams, peanuts and other crops with high economic benefits, and the agricultural economy developed more rapidly. The restructuring of industry and agriculture promoted the development of related tertiary industries (such as tourist attractions, transportation services, etc.), such as the tertiary industry correlation coefficient of 0.898 in the regression model. The output value increased from 28.903 billion in 2009 to 113.12 billion in 2019, with an average annual growth rate of 29.14%, and the rapid development of the tertiary industry also reflected the local urbanization process. For example, the construction of tourist attractions and related supporting facilities and the construction of transportation networks have expanded the urban space. Farmers have engaged in the service industry, prompting an increase in the non-farm population and the expansion of urban scale. Both of which have directly or indirectly caused an increase in the area of construction land.

(3) Social development level. The regression model shows that the rural per capita net income is highly correlated with the area of construction land, with a correlation coefficient of 0.92, which has increased by 157.9% in the past ten years. As incomes rose, large numbers of new homes began to be built in vast rural areas farther from the city. The rural scale radiated outward, causing the construction land area to increase continuously. In particular, in 2014, Jiaozuo set up an urban–rural integration demonstration zone; a large number of high-tech industries were completed and put into production. The "One body, Two wings", which was the main urban functional area, the logistics industrial zone and the ecological agricultural area, were completed. The people's income and living standards in the villages and towns in the region increased rapidly, and some villages and towns began to take on an urban scale. This process and the development of related derivative service industries have increased the total retail sales of consumer goods in the region, and accelerated the urbanization process of Jiaozuo as a whole.

4. Discussion

This manuscript builds the R-IMNet model based on the 3D-2D-CNN convolutional neural network. The "intelligent module", which can selectively emphasize the informational characteristics, is introduced through the residual link. It overcomes the problems of low classification accuracy and the loss of the edge information of objects. However, Jiaozuo is located at the junction of the Taihang Mountains area and the Yellow River alluvial plain. It is still difficult to classify by R-IMNet because of its dense population and disordered land use structure in the transition zone between the mountain area and the plain. Moreover, the spatial resolution of the image data used in this study is not high. Some small objects are difficult to be imaged. Therefore, it has an impact on the classification results. A small sample classification model is established to ensure the correct rate of samples. By reducing the probability of wrong samples participating in the training model, the accuracy of classification results can be further improved to meet the requirements of subsequent quantitative analysis.

This study mainly analyzes the impact of socio-economic factors on the evolution of regional land use, and obtains the key driving factors. Urban transformation, and industrial and agricultural restructuring in the study area play an indispensable role in the overall regional land structure transformation process, such as implementing some

special engineering measures and land use policies during the transformation process [59]. During the study period, the rapid economic development and continuous urbanization of Jiaozuo directly led to the decrease in cultivated land area (690.97 km^2) and the increase in construction land area (839.38 km^2). Some studies have shown that the loss of cultivated land has been slowed down to a certain extent by the national policy of cultivated land requisition and compensation and essential farmland protection [60]. At the same time, the government of Jiaozuo invested a lot of money to carry out land remediation work in the mining sinkhole area and to plant trees, which led to the transformation of some bare land into forest land. In addition, the policy of returning farmland to forest has also led to the conversion of some cultivated land into forest land. This manuscript mainly discusses the influence of socio-economic and policy factors on regional land change, excluding the influence of natural factors such as temperature, precipitation and slope. Still, it cannot be denied that these natural factors also play an important role in regional land change.

Compared with the driving forces of land change in other regions, the land use change in Jiaozuo is greatly affected by economic and policy factors. For example, in the Loess Plateau, the country's strict implementation of the "returning farmland to forest" policy has resulted in a continuous increase in the forest area [43]. In the southern part of Jiangsu Province, China, its developed economy attracts many people every year, resulting in urban expansion and dramatic changes in land use structure [61]. However, Jiaozuo is not as economically developed as the southern part of Jiangsu Province. The main impact of economic development is the government's fixed asset investment and per capita net income of farmers, and the implementation of policies is not as strict as the Loess Plateau. Therefore, the factors that affect the change in land use in Jiaozuo have their particularities. That is, it is influenced by a combination of factors, rather than a single factor that dominates.

Regional land use conversion may become more frequent with the dual impact of urban transformation and accelerated urbanization in Jiaozuo. However, due to the country's strict farmland protection policy, the large-scale land conversion will not occur in the future. Moreover, the driving factors of changes in the same land use type may differ in different regions, and the driving factors of changes in different land use types in the same region also differ. Therefore, in order to formulate scientific, reasonable and sustainable land use policy, it is necessary to analyze the driving factors of specific land use type change and study the land use evolution process from a microcosmic scale [44]. This can help to reveal the interaction between the biophysical environment and human activities. In this way, it is possible to better coordinate the relationship between urban development and land use, ease the contradiction between human and land, and make land conversion within a reasonable range.

5. Conclusions and Prospects

In this study, a hybrid convolutional neural network algorithm is proposed to overcome the problems of low classification accuracy and missing edge information in traditional methods. On this basis, the land use classification of the four periods of Landsat image data in Jiaozuo was carried out, and the land use data with high accuracy in the study area were obtained. Furthermore, the spatial and temporal pattern of land use transfer in Jiaozuo was discussed based on land use dynamic attitude, land use structure information entropy and land use transfer matrix. The results show that during the study period, the land use types in Jiaozuo were mainly woodland, cultivated land and construction land, which accounted for more than 90% of the total area of the study area. Among them, the area of woodland, cultivated land, water body and other land was reduced, and the area of construction land increased. From 1993 to 2020, the most drastic changes were observed in cultivated land and construction land, with area changes of -690.97 km^2 and 839.38 km^2, respectively. The information entropy of land use structure increased from 1.24 to 1.31, which indicates that the land use was in a state of rapid change and the instability of the whole system increased.

According to the land use transfer matrix and transfer mapping, it can be seen that: during 1993–2020, cultivated land was the primary type of transfer out, and its conversion object was mainly construction land. The cultivated land was transformed into 201.89 km^2, 344.14 km^2 and 374.92 km^2, respectively, in the three periods. Woodland, bare land, water body and other land all had changes of transfer in and out. A large amount of woodland was transferred from 1993 to 2003, with a conversion area of 281.23 km^2 and a conversion rate of 36.2%. From 2003 to 2011, many conversions occurred on land other than cultivated land, with a conversion rate of 87.19%. In 2011–2020, the transfer of woodland occurred and recovered to the level of 1993. In addition to cultivated land, bare land and water body also showed a large transfer out, 202.18 km^2 and 42.63 km^2, respectively, with a transfer out rate of 94.65% and 72.61%. The magnitude of land use conversion was more drastic in the urban–rural interface and the overland area between settlements and non-residents.

An analysis of the drivers of land use change in Jiaozuo showed that: policy factors and social development level affect the process of land evolution in the study area together; their cumulative contribution rate was 94.62%. The positioning of the "resource-exhausted city" has prompted the local government to adjust the industrial structure and change the land use pattern. The rapid growth in the tertiary sector of the economy and the increase in rural per capita net income have led to the expansion of urban areas and the increase in self-built rural housing, both of which have led to the conversion of cultivated land to construction land. The cultivated land protection policy and land remediation engineering measures have alleviated the decrease in quantity to a certain extent. With the continuous urbanization of Jiaozuo and the improvement in people's economic income, the people's awareness of the intensive and economical use of land has increased. At the same time, the contradiction between man and land has been eased.

Finally, we hope that this study can provide a certain reference for the local government and other similar cities in the world to carry out land use planning under the premise of ensuring food security, rationally developing and utilizing land, and properly handling the relationship between people and land, so that there is regional land use evolution of a reasonable scope.

Author Contributions: Conceptualization, C.W.; methodology, Y.Z.; project administration, C.W. and X.W.; supervision, X.W. and H.Q.; writing—original draft, Y.Z.; writing—review and editing, C.W., Y.Z., J.W., X.W., W.Y. and B.L. All authors have read and agreed to the published version of the manuscript.

Funding: Henan Provincial Science and Technology Research Project (222102110038, 222102210131); Japan Society for the Promotion of Science (JSPS) KAKENHI Grant (No. 20K12146); Henan Polytechnic University Doctoral Fund Project (B2021-19).

Data Availability Statement: Not applicable.

Acknowledgments: We appreciate the technical support of the Geospatial data cloud site.

Conflicts of Interest: We declare that the research was conducted in the absence of any commercial or financial relationships that could be construed as a potential conflict of interest.

References

1. Zhang, K.; Yu, Z.; Li, X. Land use change and land degradation in China from 1991 to 2001. *Land Degrad. Dev.* **2007**, *18*, 209–219. [CrossRef]
2. Ellis, E.C. Anthropogenic transformation of the terrestrial biosphere. *Philos. Trans. R. Soc. A Math. Phys. Eng. Sci.* **2011**, *369*, 1010–1035. [CrossRef] [PubMed]
3. González, M.; Martínez, M.G.; Lithgow, D. Land use change and its effects on the value of ecosystem services along the coast of the Gulf of Mexico. *Ecol. Econ.* **2012**, *82*, 23–32. [CrossRef]
4. Portela, R.; Rademacher, I. A dynamic model of patterns of deforestation and their effect on the ability of the Brazilian Amazonia to provide ecosystem services. *Ecol. Model.* **2001**, *143*, 115–146. [CrossRef]
5. Verburg, P.H.; Overmars, K.P. Combining top-down and bottom-up dynamics in land use modeling: Exploring the future of abandoned farmlands in Europe with the Dyna-CLUE model. *Landsc. Ecol.* **2009**, *24*, 1167. [CrossRef]

6. Zhang, W.L.; Liu, Q.; Wu, C.B. Annual change detection of land use status based on twin neural networks. *Mapp. Bull.* **2021**, *0*, 91–95, 104.
7. Randazzo, G.; Cascio, M.; Fontana, M.; Gregorio, F.; Lanza, S.; Muzirafuti, A. Mapping of Sicilian Pocket Beaches Land Use/Land Cover with Sentinel-2 Imagery: A Case Study of Messina Province. *Land* **2021**, *10*, 678. [CrossRef]
8. Waśniewski, A.; Hościło, A.; Chmielewska, M. Can a Hierarchical Classification of Sentinel-2 Data Improve Land Cover Mapping? *Remote Sens.* **2022**, *14*, 989. [CrossRef]
9. Rozenstein, O.; Karnieli, A. Comparison of methods for land-use classification incorporating remote sensing and GIS inputs. *Appl. Geogr.* **2011**, *31*, 533–544. [CrossRef]
10. Zhang, Y.; Yang, H.; Yuan, C. A review of remote sensing image classification methods. *J. Arms Equip. Eng.* **2018**, *39*, 108–112.
11. Farid, M.; Lorenzo, B. Classification of hyperspectral remote sensing images with support vector machines. *IEEE Trans. Geosci. Remote Sens.* **2004**, *42*, 1778–1790.
12. Liu, H.J.; Yang, H.X.; Xu, M.Y. Soil classification based on multi-temporal remote sensing image features and maximum likelihood method during bare soil period. *J. Agric. Eng.* **2018**, *34*, 132–139, 304.
13. Hou, M.J.; Yin, J.P.; Ge, J. A remote sensing classification method for land cover in alpine wetland areas based on random forest. *J. Agric. Mach.* **2020**, *51*, 220–227.
14. Mariana, B.; Lucian, D. Random forest in remote sensing: A review of applications and future directions. *ISPRS J. Photogramm. Remote Sens.* **2016**, *114*, 24–31.
15. Mana, S.; Robert, B. Land-use scene classification: A comparative study on bag of visual word framework. *Multimed. Tools Appl.* **2017**, *76*, 23059–23075.
16. Bhabesh, D.; Helal, M.; Avv, P. Fast Multispectral Image Super-resolution via Sparse Representation. *IET Image Process.* **2020**, *14*, 2833–2844.
17. Zou, Q.; Ni, L.H.; Zhang, T. Deep learning based feature selection for remote sensing scene classification. *IEEE Geosci. Remote Sens. Lett.* **2015**, *12*, 2321–2325. [CrossRef]
18. Zhang, L.; Zhang, L.; Du, B. Deep learning for remote sensing data: A technical tutorial on the state of the art. *IEEE Geosci. Remote Sens. Mag.* **2016**, *4*, 22–40. [CrossRef]
19. Zhu, X.X.; Tuia, D.; Mou, L. Deep learning in remote sensing: A comprehensive review and list of resources. *IEEE Geosci. Remote Sens. Mag.* **2017**, *5*, 8–36. [CrossRef]
20. Kussul, N.; Lavreniuk, M.; Skakun, S. Deep learning classification of land cover and crop types using remote sensing data. *IEEE Geosci. Remote Sens. Lett.* **2017**, *14*, 778–782. [CrossRef]
21. Wang, B.; Fan, D.L. Summary of research progress of deep learning in remote sensing image classification and recognition. *Bull. Surv. Mapp.* **2019**, *2*, 99–102.
22. Li, S.T.; Song, W.W.; Fang, L.Y.; Chen, Y.; Ghamisi, P.; Benediktsson, J.A. Deep learning for hyperspectral image classification: An overview. *IEEE Trans. Geosci. Remote Sens.* **2019**, *57*, 6690–6709. [CrossRef]
23. Li, X.J.; Yang, G.H. Adaptive fault-tolerant synchronization control of a class of complex dynamical networks with general input distribution matrices and actuator faults. *IEEE Trans. Neural Netw. Learn. Syst.* **2017**, *28*, 559–569. [CrossRef] [PubMed]
24. Han, X.P.; Zhong, Y.F.; Zhao, B. Scene classification based on a hierarchical convolutional sparse auto encoder for high spatial resolution imagery. *Int. J. Remote Sens.* **2016**, *38*, 514–536. [CrossRef]
25. Maggiori, E.; Tarabalka, Y.; Charpiat, G. Fully convolutional neural networks for remote sensing image classification. In Proceedings of the 2016 IEEE International Geoscience and Remote Sensing Symposium (IGARSS), Beijing, China, 10–15 July 2016; pp. 5071–5074.
26. Zhang, Y.; Zhang, E.; Chen, W.J. Deep neural network for halftone image classification based on sparse autoencoder. *Eng. Appl. Artif. Intell.* **2016**, *50*, 245–255. [CrossRef]
27. Mou, L.C.; Bruzzone, L.; Zhu, X.X. Learning spatial-temporal features via a recurrent convolutional neural network for change detection in multispectral imagery. *IEEE Trans. Geosci. Remote Sens.* **2019**, *57*, 924–935. [CrossRef]
28. Zhang, M.Y.; Xu, G.L.; Chen, K. Triplet-based semantic relation learning for aerial remote sensing image change detection. *IEEE Geosci. Remote Sens. Lett.* **2019**, *16*, 266–270. [CrossRef]
29. Liu, R.C.; Cheng, Z.H.; Zhang, L.L. Remote sensing image change detection based on information transmission and attention mechanism. *IEEE Access.* **2019**, *7*, 156349–156359. [CrossRef]
30. Gong, M.G.; Zhao, J.J.; Liu, J. Change detection in synthetic aperture radar images based on deep neural networks. *IEEE Trans. Neural Netw. Learn. Syst.* **2017**, *27*, 125–138. [CrossRef]
31. Lee, H.; Kwon, H. Going Deeper with Contextual CNN for Hyperspectral Image Classification. *IEEE Trans. Image Process.* **2017**, *26*, 4843–4855. [CrossRef]
32. Swalpa, K.R.; Shiv, R.D.; Subhrasankar, C. FuSENet: Fused squeeze-and-excitation network for spectral-spatial hyperspectral image classification. *IET Image Process.* **2020**, *14*, 1653–1661.
33. Yang, M. Hyperspectral Image Classification Based on Attention and Feature Convolutional Neural Network. Ph.D. Thesis, Xidian University, Xi'an, China, 2020.
34. Qin, A.Y.; Zhao, W. Spectral–Spatial Graph Convolutional Networks for Semi-supervised Hyperspectral Image Classification. *IEEE Geosci. Remote Sens. Lett.* **2018**, *16*, 241–245. [CrossRef]

35. Wan, S.; Gong, C.; Zhong, P. Multi-scale Dynamic Graph Convolutional Network for Hyperspectral Image Classification. *IEEE Trans. Geosci. Remote Sens.* **2019**, *58*, 3162–3177. [CrossRef]
36. Fang, J.J.; Sha, J.M.; Zhou, Z.L. Random forest based land use change and urban driven analysis. *Comput. Syst. Appl.* **2021**, *30*, 12–20.
37. Yang, H.Y.; Zhu, X. Impact of metro construction on spatial and temporal changes of urban land use. *Intell. Build. Smart Cities* **2020**, *37*, 31–34.
38. Jiang, W.J.; Lin, M.H.; Weng, P.Y. Analysis of spatial and temporal land use evolution patterns and their key drivers in Anxi County, Fujian Province. *J. Ecol.* **2022**, *42*, 513–527.
39. Yu, C.L.; Wang, C.C.; Liu, D. Evolutionary process and driving force analysis of natural wetlands in West Liaoning River Basin based on SWAT model. *J. Agric. Eng.* **2020**, *36*, 286–297.
40. Kamwi, J.M.; Cho, M.A.; Kaetsch, C. Assessing the Spatial Drivers of Land Use and Land Cover Change in the Protected and Communal Areas of the Zambezi Region, Namibia. *Land* **2018**, *7*, 131. [CrossRef]
41. Kamwi, J.M.; Chirwa, P.W.C.; Manda, S.O.M. Livelihoods, land use and land cover change in the Zambezi Region, Namibia. *Popul. Environ.* **2015**, *37*, 207–230. [CrossRef]
42. Imbernon, J. Pattern and development of land-use changes in the Kenyan highlands since the 1950. *Agric. Ecosyst. Environ.* **1999**, *76*, 67–73. [CrossRef]
43. Huang, H.; Zhou, Y.; Qian, M. Land Use Transition and Driving Forces in Chinese Loess Plateau: A Case Study from Pu County, Shanxi Province. *Land* **2021**, *10*, 67. [CrossRef]
44. Jiaozuo People's Government Website. Available online: http://www.jiaozuo.gov.cn/ (accessed on 18 July 2019).
45. Wang, X.P.; Qi, H.W.; Xie, H. A preliminary investigation on the development pattern of geological environmental problems of mines in resource-depleted cities in Jiaozuo. *China Resour. Compr. Util.* **2020**, *38*, 144–146.
46. Lu, D.; Weng, Q. A survey of image classification methods and techniques for improving classification performance. *Int. J. Remote Sens.* **2007**, *28*, 823–870. [CrossRef]
47. Liu, J.Y.; Zhang, Z.X.; Xu, X.L. Spatial patterns and driving forces of land use change in China during the early 21st century. *J. Geogr. Sci.* **2010**, *20*, 483–494. [CrossRef]
48. Song, W.; Deng, X.Z. Land-use/land-cover change and ecosystem service provision in China. *Sci. Total Environ.* **2017**, *576*, 705–719. [CrossRef]
49. Guo, Z.S.; Li, C.H.; Wang, Z.M. Road extraction from ZY-3 remote sensing image based on U-Net like convolution architecture. *Sci. Surv. Mapp.* **2020**, *45*, 51–57.
50. Sang, X.; Guo, Q.Z.; Pan, Y.Y. Research on land use dynamic change and prediction in Lucheng City of Shanxi Province based on TM and OLI. *Remote Sens. Land Resour.* **2018**, *30*, 125–131.
51. Li, Q.P.; Lu, R.C.; Liang, B.K. Construction of land use information mapping in land border areas of Guangxi. *Soil Water Conserv. Res.* **2016**, *23*, 210–215.
52. Wen, W.D. Analysis of industrial restructuring in resource-based cities—Jiaozuo City as an example. *J. Henan Univ.* **2002**, *2*, 84–87.
53. Guo, P.; Zhou, W.; Yuan, T. Analysis of spatial and temporal changes in land use and driving factors in declining resource cities. *Soil Water Conserv. Res.* **2016**, *23*, 191–198.
54. Zhong, H.X. The chronic problem of illegal mining in Jiaozuo City, Henan Province is difficult to be eliminated. *China Environ. Monit.* **2021**, *5*, 72–74.
55. Li, R.P.; Lu, X.H. A study on the expansion of rural residential bases and the driving mechanism. In Proceedings of the 2009 Annual Academic Conference of the Chinese Land Institute Anhui Procince, Hefei, China, 19 December 2009; pp. 45–51.
56. Anonymous. "The 2017 Air Pollution Prevention and Control Work Program for Beijing, Tianjin, Hebei and Surrounding Areas" Released. *Environ. Dev.* **2017**, *29*, 4.
57. Xu, C.L.; Ji, P.Y.; Gong, W.F. Land use change characteristics and driving forces analysis in counties of southwest China from 2000-2015–Fengjie County, Chongqing, as an example. *China Agron. Bull.* **2021**, *37*, 98–107.
58. Chang, C.; Liu, X.; Chang, G.C.; Yao, X.Y. Chang Ronghua, Chang Rong. Land Use Dynamics and driving forces of cultivated land change in Mengyin County. *Sci. Soil Water Conserv. China* **2010**, *8*, 65–70.
59. Müller, D.; Kuemmerle, T.; Rusu, M. Lost in transition: Determinants of post-socialist cropland abandonment in Romania. *J. Land Use Sci.* **2009**, *4*, 109–129. [CrossRef]
60. Qian, F.; Chi, Y.; Lal, R. Spatiotemporal characteristics analysis of multifunctional cultivated land: A case-study in Shenyang, Northeast China. *Land Degrad. Dev.* **2020**, *31*, 1812–1822. [CrossRef]
61. Guo, Y.H. A study on land use changes and socio-economic drivers in economically developed regions—Taking the southern Jiangsu region as an example. *Urban Geogr.* **2017**, *10*, 30–31.